

EFFECT OF SINTERING TEMPERATURE ON MICROSTRUCTURE AND *IN-VITRO* BEHAVIOR OF BIOACTIVE GLASS-CERAMICS

#M. U. HASHMI*, SAQLAIN A. SHAH**, F. UMER***, ASHRAF S. ALKEDY****

*Department of Applied Sciences, Superior University, Lahore, Pakistan

**Department of Physics, Forman Christian College, Lahore, Pakistan

***Department of Basic Sciences, UMT, Sialkot, Pakistan

****Department of Physics, King Abdulaziz University, Jeddah, KSA,
Egyptian Atomic Energy Authority (EAEA), Cairo, Egypt

#E-mail: usmanhashmi06@hotmail.com

Submitted April 5, 2013; accepted November 28, 2013

Keywords: Oxy-acetylene blue flame, Hydroxyapatite HA, Wollastonite, Diameter shrinkage co-efficient, Density

In this work, powders of the composition (CaO 46- SiO₂ 34- P₂O₅ 14.5- MgO 4- CaF₂ 1- MgF₂ 0.5) (wt. %) were thoroughly mixed and melted in a muffle furnace. The melt was quenched in water to form glass. Three glass-ceramics were prepared by sintering glass samples at three different temperatures 850, 900 and 950°C according to the exothermal peaks of DTA. The DTA peaks correspond to the bioactive crystalline phases hydroxyapatite(HA) and wollastonite as confirmed by the XRD data. Study of diameter-shrinkage co-efficient and bulk-density of samples revealed higher densification rate for the range 900 - 950°C than that for the range 850 - 900°C. SEM and optical microscope results illustrated a tendency towards closely packed structure and increasing grain size with the increase of sintering temperature. The samples were immersed in SBF for 30 days at room temperature for in-vitro evaluation. EDS analysis, showing the presence of carbon(C) along with calcium(Ca) and phosphorus(P) suggests the formation of hydroxycarbonate-apatite(HCA) phase that indicates the bioactivity of the material which increases with the increase of sintering temperature.

INTRODUCTION

Glass-ceramics are the polycrystalline solid materials prepared by the controlled crystallization of parent glasses according to the desired set of biological, structural and mechanical properties [1]. Bioactive glass-ceramics own the ability to make a bond with the bone tissues in physiological environment [2]. Bioactivity of glass-ceramics is measured by the rapidity of development of hydroxycarbonate apatite (HCA) and its bonding with the surrounding tissues [3]. The well known bioactive glass-ceramics in orthopedics applications are calcium phosphate based hydroxyapatite containing glass-ceramics having chemical resemblance to the inorganic component of bone and teeth. Small variations in Ca/P ratios of calcium phosphate glass ceramics cause to change the structural and biodegradation behavior of the glass ceramics [4]. Apatite-wollastonite containing glass-ceramics (A-W GC) are also well known for having *in-vitro* and *in-vivo* stability and are difficult to be resolved in physiological fluids [5]. Bioactive glass-ceramics containing apatite and wollastonite phases are found to have good mechanical properties like bending strength, fracture toughness and young's modulus etc, enabling to be used in load bearing applications such as vertebral prostheses etc [6-10]. Bioactivity and microstructure of glass-ceramics are found to vary by compositional changes and changes of preparation parameters [6,11].

Research is in progress on the preparation, microstructure characterization and biological evaluation of bioactive glass-ceramics [12-18] and there is a great need to prepare new bioactive glass-ceramics using every possible compositional changes and changes of preparation parameter because bioactivity and microstructure properties of glass-ceramics are found to be greatly affected by these important variations. The present investigation is an attempt to prepare bioactive glass-ceramics of the system (CaO 46- SiO₂ 34- P₂O₅ 14.5- MgO 4- CaF₂ 1- MgF₂ 0.5) (wt. %) by melting the thoroughly mixed powders in a muffle furnace and sintering the glass powders at different temperatures according to the DTA data. Microstructure characterization is carried out employing thermal analysis using differential thermal analyzer, crystallization studies using X-ray diffraction, bulk densification and surface morphological studies using scanning electron microscope. Energy dispersive spectrum is used to investigate the *in-vitro* behavior of the glass-ceramic samples after immersion in SBF for thirty days.

EXPERIMENTAL

Sample Preparation

Figure 1 shows the flow chart for the preparation of bioactive glass-ceramics. Thoroughly mixed powders of the composition (CaO 46- SiO₂ 34- P₂O₅ 14.5- MgO

4- CaF₂ 1- MgF₂ 0.5) (wt. %) were melted in a muffle furnace at 1500°C in a platinum crucible and the melt was quenched in water to form glass. The glass was powdered using agate mortar and pestle for several hours and compacted under a pressure of 10⁸ Pa in a hydraulic press. 5 wt. % polyvinyl alcohol (PVA) was used as organic binder for compaction. The glass compacts were sintered at 850, 900 and 950°C for three hours according to the exothermal peaks of DTA data, in a muffle furnace operating at the ramp rate of 5°C/min. The samples were maintained at 700°C for 1 hour for the creation of nucleation sites before crystallization. The samples were named as GC1, GC2 and GC3 respectively according to sintering temperatures.

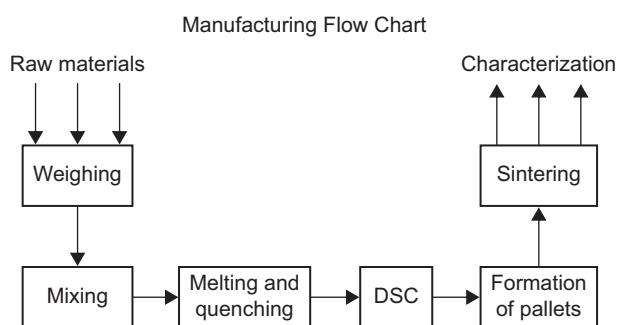


Figure 1. Flow chart of preparation of glass ceramics.

Sample Characterization

Thermal analysis was carried out on glass powder using DTA apparatus (SDT Q600 V8.0 Build 95) from room temperature to 1400°C with ramp rate of 5°C/min. Microstructure characterization of the samples was performed by X-ray diffraction (Panalytical X'Pert PRO MPD θ - θ X-Ray Diffractometer) using Cu K α 1 radiation ($\lambda = 1.54056 \text{ \AA}$) and data was evaluated using X'Pert high score software.

Morphological study of the samples was performed by optical microscopy (Leica DM 4000) and scanning electron microscopy (JEOL, JSM 840A) using secondary electron mode of imaging.

To study the densification behavior, diameter shrinkage co-efficient was determined by plotting a slope of diameter shrinkage vs temperature and density was calculated by using Archimedes equation.

Bioactivity of samples was investigated by immersing the samples in simulated body fluid for thirty days at 37°C. EDS was used for *in-vitro* characterization.

RESULTS AND DISCUSSION

Thermal Analysis

Figure 2 shows the DTA curves of glass. High glass transition temperature T_g (730°C) indicates the closely packed structure and thermal stability of the glass system

[19]. The regular crystallization process begins at 850°C which achieves saturation at 870°C indicated by the exothermic peak, attributed to the crystallization of HA phase, which also suggests the upper temperature limit of the thermal stability of the glass [20]. The second exotherm at 960°C corresponds to the crystallization of wollastonite phase as confirmed by the XRD results.

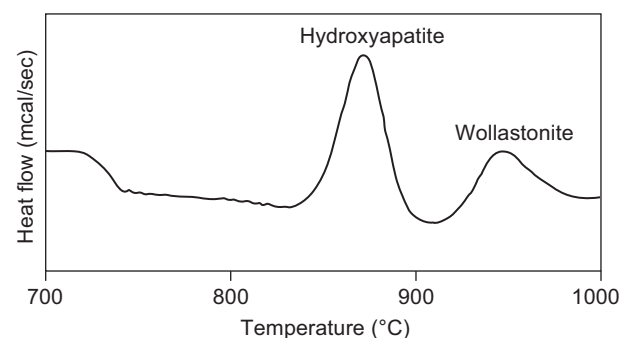


Figure 2. DTA graph of glass powder.

XRD Analysis

Figure 3 shows the XRD graphs of glass-ceramic samples GC1, GC2 and GC3. Crystalline phases of hydroxyapatite (HA) Ca₁₀(PO₄)₃(OH)₂ are the most prominent with minor phases of wollastonite (CaO-Si₂O) in the graph of GC1. Graph of GC2 shows the slight increase in peak intensities with the rise in sintering temperature indicating the crystals growth. Formation of wollastonite phases is much prominent in the graph of GC3 showing the proficient growth of wollastonite at the sintering temperature 950°C as confirmed by DTA graph. The graph of peak intensities of dominant phases vs temperature is shown in Figure 4. The average crystallite size was calculated using Scherrer's formula [3]:

$$\text{Crystallite size} = 0.89\lambda / \text{FWHM} \cos \theta$$

where $\lambda = 1.54 \text{ \AA}$ is the wavelength of the X-ray, FWHM is the full width at half maxima (in radian) of the particular diffraction peak and θ is the corresponding

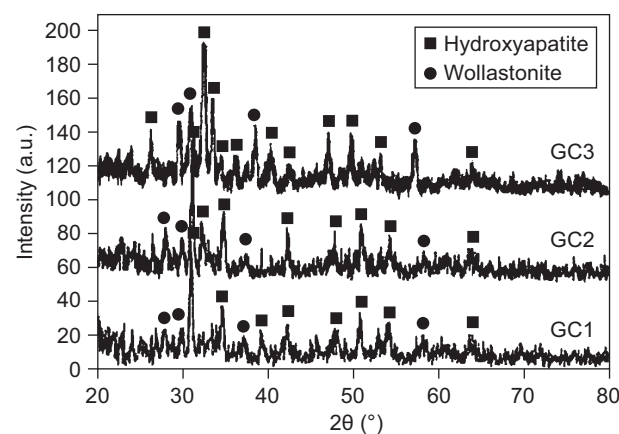


Figure 3. XRD graphs of samples GC1, GC2 and GC3.

Bragg's angle of the diffraction peak. The crystallite size (Figure 5) of HA increases uniformly from 34.7 nm to 35.1 nm with the sintering temperature and that of wollastonite enlarges from 23.2 nm to 23.4 nm in the temperature range (850 - 900°C) and then from 23.4 nm to 24.1 nm in the temperature domain (900 - 950°C), showing the larger crystal growth of wollastonite which is in accordance with the DTA data.

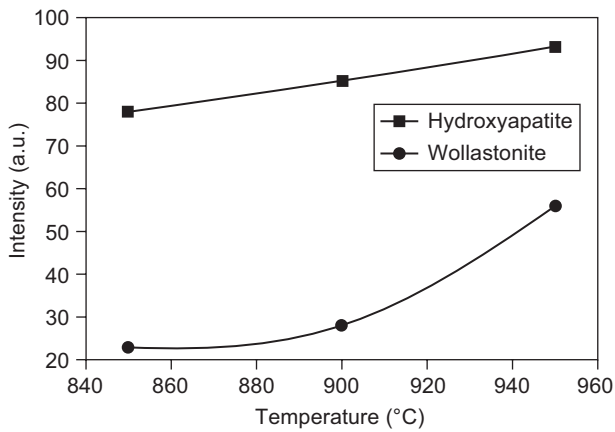


Figure 4. Graph of peak intensity vs. sintering temperature.

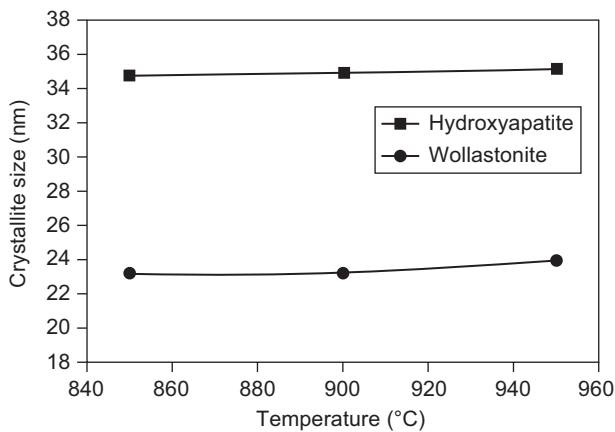


Figure 5. Graph of crystallite size vs. sintering temperature.

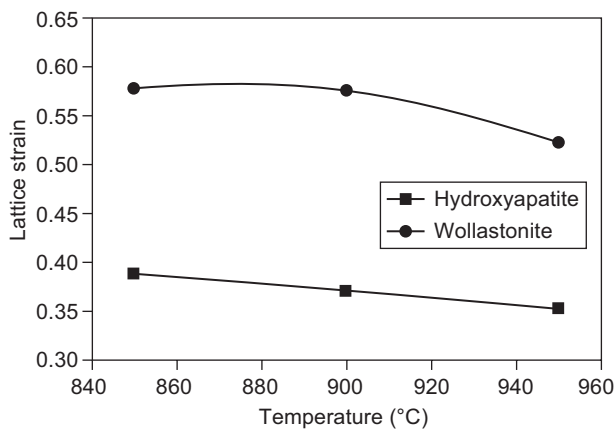


Figure 6. Graph of lattice strain vs. sintering temperature.

Slight phase shifting occurs in GC2 which is more prominent in GC3 due to the internal stresses which may have originated due to the lattice distortions caused by the incorporation of impurity atoms of different radii at the lattice sites at higher temperatures [21]. Lattice distortion or strain was calculated by the X'pert high score software. It varied inversely to the crystallite size against the sintering temperature as shown in Figure 6.

Densification of the samples

Behavior of diameter shrinkage of the samples with the sintering temperature (Figure 7) was examined using the formula:

$$\text{Diameter Shrinkage} = \Delta D/D_0 = (D - D_0)/D_0$$

where D is measured diameter of sample at temperature T and D_0 is the diameter of the sample at ambient temperature. Diameter shrinkage co-efficient α , determined by plotting a slope of $\Delta D/D_0$ vs temperature is shown in Figure 8.

Graphs of Figures 7 and 8 suggest the increasing densification process by the reduction of pores and diffusion of the particles along the grain boundaries at

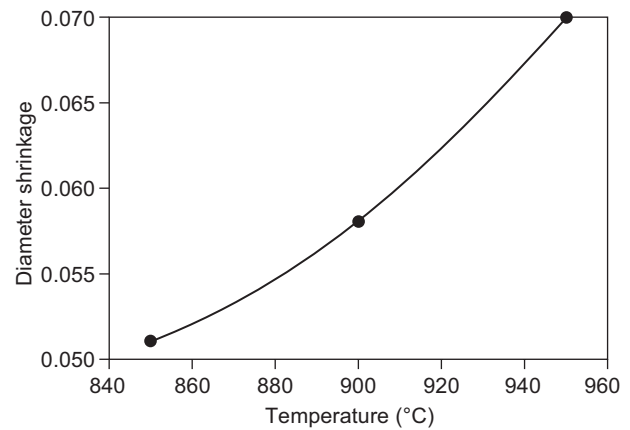


Figure 7. Graph of diameter shrinkage vs sintering temperature.

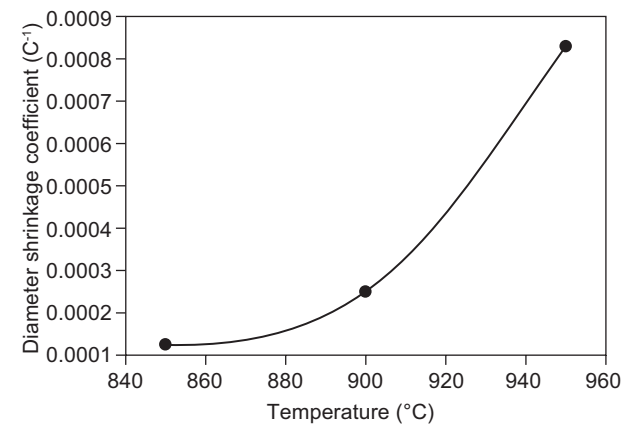


Figure 8. Graph of diameter shrinkage coefficient vs sintering temperature.

higher temperatures. Rate of densification was higher for the temperature domain (900 - 950°C) than that for (850 - 900°C) because in lower range the crystallization of hydroxyapatite phase was prominent but in the higher temperature range, both the hydroxyapatite and wollastonite crystallization contributed to the greater densification process thus increasing the bulk density in the higher temperature domain as shown in Figure 9.

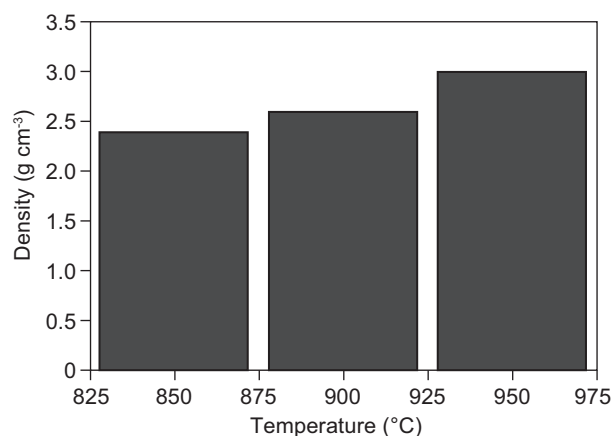


Figure 9. Graph of bulk density vs. sintering temperature.

Densities of all the samples were measured by Archimedes equation [19]:

$$\rho = a * \rho_w / (a - b)$$

where ρ = density of sample, a = weight of sample in air, b = weight of sample in liquid, ρ_w = density of water.

Change in density from 850 - 900°C is found to be 2.4 g/cm³ to 2.6 g/cm³ whereas from 900 - 950°C that is 2.6 g/cm³ to 2.9 g/cm³ showing the higher densification at higher temperature as conformed by optical microscopy and scanning electron microscopy. This change in densities against temperature is shown in Figure 9.

Optical microscopy

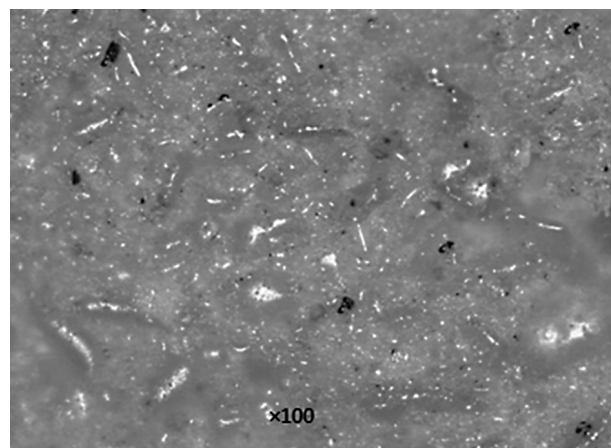
Optical microscopy for the surface morphology was carried out for each sample at 100 times magnification. The small glazed regions in the micrographs show the glassy matrix with fine crystals embedded in it as shown in Figures 10a, 10b and 10c. The red spots in the micrographs are associated with the hydroxyapatite crystals. An increase in the grain growth is observed by increasing the sintering temperature.

Scanning electron microscopy

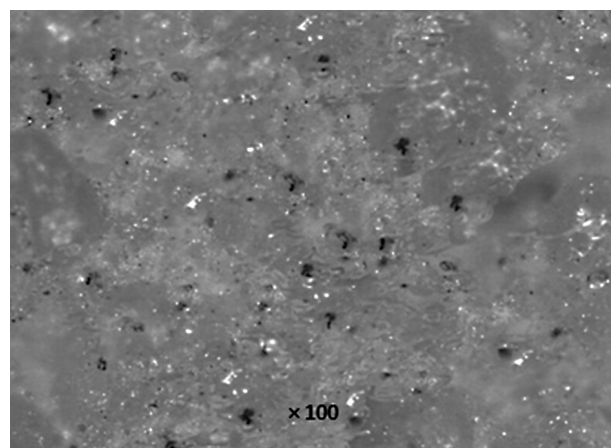
Figures 11a, 11b and 11c are the scanning electron micrographs showing the magnified images of GC1, GC2 and GC3 respectively.

Small grains are attributed to wollastonite and larger grains are of hydroxyapatite. Micrographs of GC2 and GC3 show that grains are being closely packed and

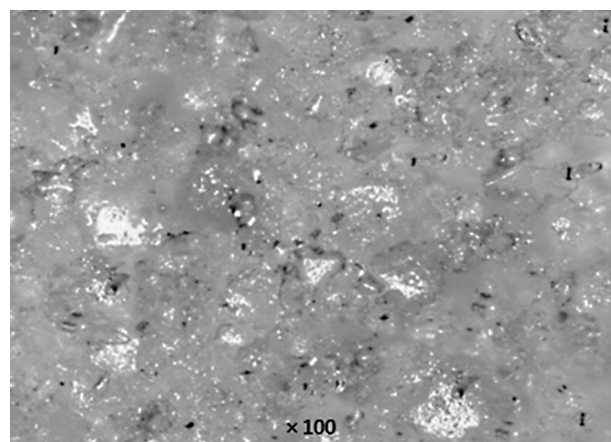
their densification increases by increasing the sintering temperature that may be due to the efficient migration of the materials from grain boundaries between the particles thus forming necks and gradual elimination of vacancies at the surface at higher temperature [3]. This behavior is highly visible in GC3 due to greater atomic motion and enhancement in crystalline size of wollastonite at higher temperature.



a) GC1

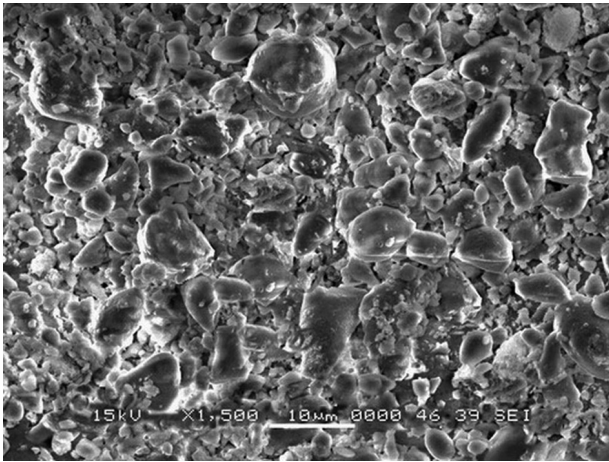


b) GC2

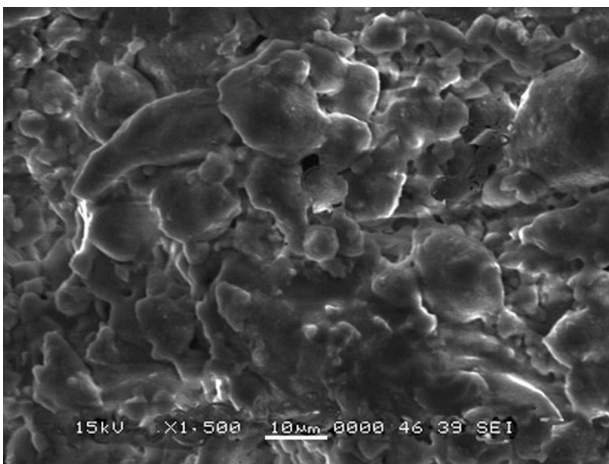


c) GC3

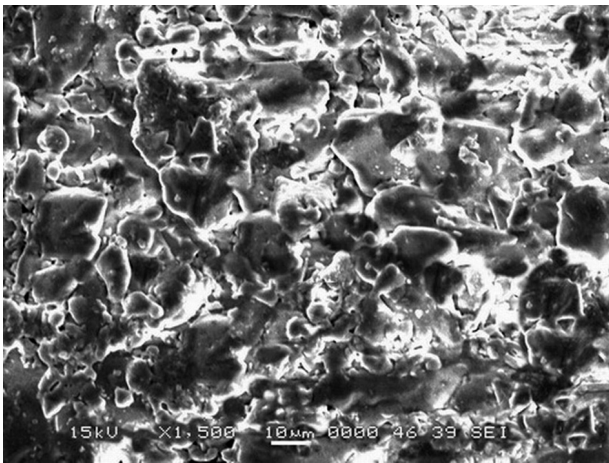
Figure 10. Optical micrograph of sample GC1 (a), GC2 (b) and GC3 (c).



a) GC1



b) GC2



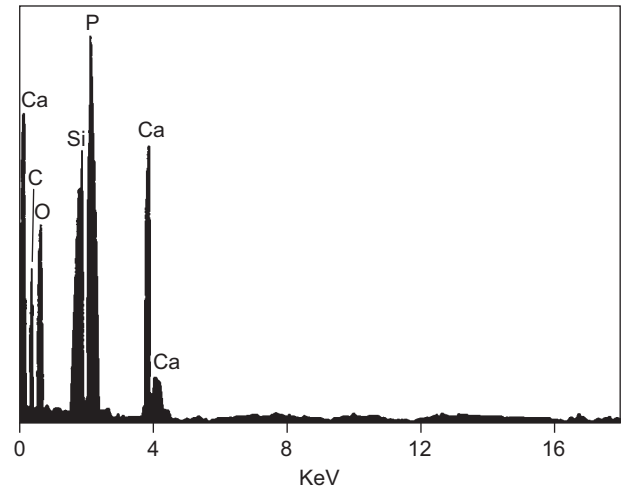
c) GC3

Figure 11. SEM micrograph of sample GC1 (a), GC2 (b) and GC3 (c).

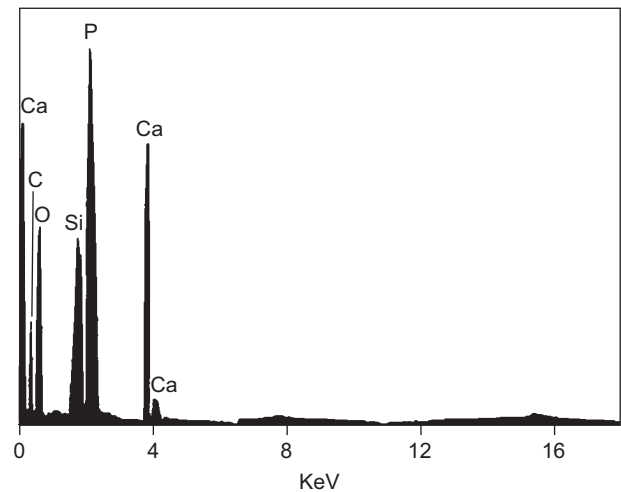
In vitro characterization

After immersion of the samples (GC1, GC2 and GC3) in the simulated body fluid for 30 days at 37°C, EDS (Figures 12a, 12b, 12c) confirms the bioactivity of all the samples by showing the presence of carbon along with Ca and P which corresponds to formation

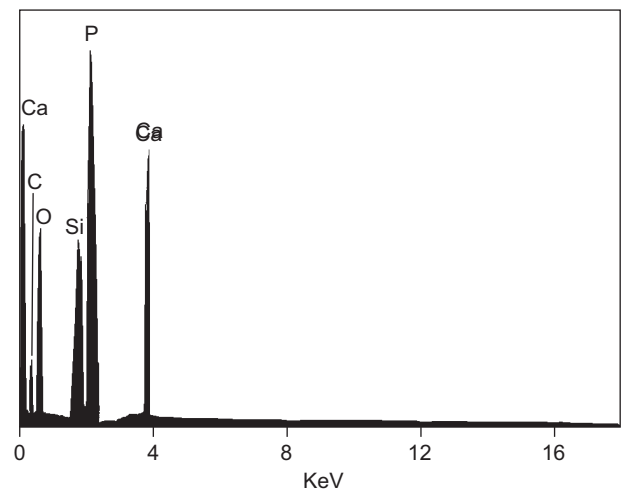
of hydroxycarbonate apatite in physiological solution. The mechanism of hydroxycarbonate apatite layer formation may be explained by the increase in saturation



a) GC1



b) GC2



c) GC3

Figure 12. EDS spectrum of GC1 (a), GC2 (b) and GC3 (c) after immersion in SBF.

of surrounding fluid owing to dissolution of Na^+ , Ca^{2+} or Si^{4+} ions from the surface of material and incorporation of CO_3^{2-} ions with OH^- ions that causes the formation of new phases on the sample's surface. EDS further reveals that bioactivity increases with the sintering temperature and it is highest for GC3.

CONCLUSIONS

1. CaO 46- SiO_2 34- P_2O_5 14.5- MgO 4- CaF_2 1- MgF_2 0.5 (wt. %) glass was prepared by conventional melt-quench method.
2. Three glass-ceramics were prepared by sintering glass samples at three different temperatures according to the DTA data of nucleation and crystallization temperatures.
3. XRD analysis of glass-ceramics samples revealed the presence of two biologically active crystalline phases, hydroxyapatite (HA) and wollastonite.
4. Crystalline phases enhanced with the increase of sintering temperature and wollastonite phase was more prominent in GC3.
5. Diameter shrinkage as well as diameter shrinkage coefficients showed the higher densification of samples in the temperature range 900 - 950°C than that in range 850 - 900°C as conformed by optical microscopy and SEM.
6. The in vitro test was performed by immersing the samples in simulated body fluid for thirty days at 37°C. EDS analysis showed the presence of carbon along with calcium and phosphorus suggesting the formation of hydroxycarbonate apatite (HCA) phases that indicates the bioactivity of the material which increases with the sintering temperature.

Acknowledgement

Authors acknowledge the cooperation of Dr. Riaz Ahmad, director of the "Centre for Advanced Studies in Physics" and support of "Higher Education Commission", Government of Pakistan. Authors are grateful

to higher authorities of Superior University Lahore and FC College Lahore for their patronage. We are also thankful to Dr. Abdul Majeed, Brooklyn Hospital Centre, Brooklyn NY U.S.A, for his technical assistance.

REFERENCES

1. Salman S. M., Salama S. N., Darwish H., Mahdy E. A.: *Ceramics International* 36, 55 (2010).
2. Hench L. L., Paschall H. A.: *J. Biomed. Mater. Res. Symposium* 7, 25 (1973).
3. Jokanovic V., Jokanovic B., Markovic D.: *Mater. Chem. Phys.* 111, 180 (2008).
4. Tas A. C., Korkusuz F., Timucin M.: *J. Mater. Sci.: Mater. in Med.* 8, 91 (1997).
5. Teramoto H., Kawai A., Sugihara S.: *Acta Medica Okayama* 59, 201 (2005).
6. Yu B., Liang K., Gu S.: *Ceram. Int.*: 28, 695 (2002).
7. Kokubo T., Shigematsu M., Nagashima Y. et al.: *Bull. Inst. Chem. Res. Kyoto Univ.* 60, 260 (1982).
8. Shyu J. J., Wu J.M.: *J. Mater. Sci. Lett.* 10, 1056 (1991).
9. Shyu J. J., Wu J. M.: *J. Am. Ceram. Soc.* 73, 1062 (1990).
10. Liu D. M., Chou H. M.: *J. Mater. Sci. Mater. Med.* 5, 7 (1994).
11. Shyu J. J., Wu J. M.: *J. Am. Ceram. Soc.* 74, 2123 (1991).
12. Laczka M., Cholewa K., Laczka-Osyczka A.: *J. Alloys Compounds* 248, 42, (1997).
13. Laczka M., Cholewa-Kowaiska K., Laczka-Osyczka A., Tworzydło M., Turyna B.: *J. Biomed. Mater. Res.* 52, 601 (2000).
14. Cornelia M., Carsten J., Christian R.: *J. Non-Cryst. Solids* 248, 169 (1999).
15. Pzriange L. M., Sims M. R.: *Eur. J. Orthod.* 15, 33 (1993).
16. Hashmi M.U., Saqlain A. Shah, Zaidi M.J.: *Ceramics-Silikaty* 56, 347 (2012).
17. Marghussian V. K., Sheikh Mehdi Mesgar A.: *Ceram. Int.* 26, 415 (2000).
18. Ma J., Chen C. Z., Wang D. G., Hu J. H.: *Ceram. Int.* 37, 1637 (2011).
19. Marikani A., maheswaran A., Premanathan M., Amalraj L.: *J. Non Cryst. Solids* 354, 3929 (2008).
20. Stoch L., Wactawska I., Ciecinska M.: *J. Therm. Analysis & Calorimetry* 65, 341 (2001).
21. Khan I. A., Hassn M., Ahmad R., Qayyum A., Murtaza G., Zakaulah M., Rawat R. S.: *Thin Solid Films* 516, 8255 (2008).